TRENDS IN SCIENCES 2025; 22(9): 10405
https://doi.org/10.48048/tis.2025.10405 RESEARCH ARTICLE

Synthesis, Structural Analysis, and Theoretical Study of Amino Acid-Copper (II) Complexes via XRD and DFT

Nahed Hazim Al-Haidery[1], Hanan Abduljaleel Al-Hazam[1] and Nuha Hussain Al-Saadawy[2,*]

[1]*Department of Chemistry, College of Science, University of Basrah, Al-Zubair, Basrah 61004, Iraq*
[2]*Department of Chemistry, College of Science, University of Thi-Qar, Nasiriyah, Thi-Qar 64001, Iraq*

([*]Corresponding author's e-mail: nuh.hussain@sci.utq.edu.iq)

Received: 19 April 2025, Revised: 25 April 2025, Accepted: 10 May 2025, Published: 5 July 2025

Abstract

New amino acid derivatives were synthesized to create copper (II) complexes, with the binding site influenced by pH levels. These complexes, derived from amino acids like alanine, histidine, tryptophan, and lysine, were characterized using various spectroscopic techniques, including IR, UV-Vis, and X-ray diffraction, which confirmed their expected crystal forms. Density functional theory (DFT) calculations were employed to analyze the electronic structures and stability of the complexes, revealing a correlation between the highest occupied molecular orbital (HOMO), lowest unoccupied molecular orbital (LUMO), energy gaps and their reactivity, thus aiding in the rational design of these compounds for applications in catalysis and biomimetic chemistry.

Keywords: Amino acid, Cu complexes, X-ray, Density Functional Theory, HOMO, LUMO, Electronic structure, Computational chemistry, Copper, Alanine, Histidine, Lysine

Introduction

Interest in the pharmacological effects of drugs and toxic effects reduction by amino acids has increased due to the role played by copper complexes. As potential pharmacological activity chelating groups, they can chelate well with groups [1,2]. In pigments anti-corrosion coatings, acids do not attack the formulation of coating on the contrary [3]. These complexes have been spectroscopically studied; Raman spectroscopy indicates that the stability constant of divalent metal ions increases with the decrease of the ionic radius of the metal ion in copper [4]. The infrared spectra of the copper complexes show the amino acids to form bidentate ligand coordination involving the carboxylic and the amino group [5]. Additional infrared studies have revealed that the main ligand dimethylglyoxime binds to the metal ion in a bidentate manner through the oxide's NN donor site [6]. The complex shows a visible circular dichroism spectrum with a strong band in the visible region at 620 ~ 490 nm. The bioinorganic chemistry of copper (II) complexes with amino acids has been a subject of growing interest because of their diverse structures, biological activities, and catalytic and medicinal applications [7]. Strong knowledge of the structural formulae is required to be able to understand coordination mode, electronic properties, and reactivity of the complexes [8]. Other than XRD that can, in a high degree, give evidence for the three-dimensional atom arrangement of such complexes, are their molecular geometry, bond lengths, and coordination modes [9]. Theoretical studies that comprise density functional theory (DFT) calculations will, by providing electronic structure, stability, and spectroscopic properties, place them in line with the experiment [10]. The combination of XRD with a theoretical study of this type will place into clear perspective all the detailed findings, bonding interactions, and ligand-field effects and magnetic properties of these complexes [11]. The crystal structure of the complex was validated by weighing the observed results for each ligand and the structure obtained by X-ray diffraction analysis [12]. This study includes the

synthesis, single-crystal XRD characterization, and theoretical investigation of copper (II) complexes based on amino acid derivatives. The above results would account for a high degree of correlation between the experimental and the computational data and thus proof of the proposed structural formulas, throwing more light on their chemical behavior [13-16]. A majority of studies have centered on amino acids and their derivatives. Most of these have been synthesized and identified as complex with transition metal ions, which includes groups with structural motifs capable of chelating these ions [17]. Diagnostics have been carried out by different techniques and their biological efficacy against fungal and bacterial species has been evidenced [18,19]. Techniques applied in the study of the chemical properties and structure of the synthesized compound include X-ray diffraction. It is considered an analysis that is non-destructive and gives information about the environment in which the crystal lies, its chemical composition, and some physical properties of materials as well as thin crystal layers [20]. This particular implementation of the technique depends on elastic X-ray scattering and is sensitive to molecular geometry. Polar radiation plots give an interpretative structural result for the complex that is formed [20,21]. DFT is rather particularly apt for a study in the middle of one of those transition metal complexes, with large electron-correlation effects. Commonly available functionals are to balance accuracy and costs of computation. i.e., M06, B3LYP, PBE [22]. The problems come in describing correctly ligand field effects, spin states, and weak interaction phenomena, for instance, dispersion forces. Recent developments in DFT, among them hybrid functionals, meta-GGA functionals, and embedding techniques have made steps forward in the applicability to systems of complexity [22]. The work "Synthesis, Structural Analysis, and Theoretical Study of Amino Acid–Copper (II) Complexes via XRD and DFT" introduces and discusses results from an integrated experimental and computational study on the coordination chemistry of copper (II) with amino acids from structural and electronic viewpoints. Herein, we report a brief novelty in its scope. Synthesis of new and known or commercially available copper(II)-amino acid complexes by any chief route and their characterization by X-ray diffraction analysis so that the bond lengths can be seen, as well as supramolecular interaction. Comparison of the quality of experimental XRD data with DFT calculations to fall in general how close the theoretical models come toward describing molecular geometry, electronic structure, and results. To study the electronic features, such as HOMO-LUMO gaps, charge sharing, and the bond character, such as Cu-N/O coordinating binding, which gives direct information on reactivity and stability. The biocatalysis, medicinal chemistry (as an antioxidant / antitumor agent), and material science-related roles of copper(II)-amino acid complexes potent structural and electronic properties for designing new functional compounds unless the above design discovers new copper(II)-amino acid complexes.

If it revisits known complexes, it is with higher-precision XRD data or advanced DFT methods, such as hybrid functionals dispersion corrections, over which there is an obvious improvement from prior work. Most studies use either experimental (XRD) or theoretical (DFT) methods. The dual approach of this work uses both to validate computational models against real-world data, enhancing reliability. The novelty of this study is in the integration of XRD and DFT to decode the structure-property relationships of Cu(II)-amino acid complexes, which may be able to bring out actual coordination motifs or validate theoretical models for future studies. Its application may find use in areas such as bioinorganic chemistry and materials science.

Materials and methods

Experimental section

^{1}H NMR spectra were recoded using BRUEK spectrophotometer 400 MHz (University of Isfahan, Iran) The chemical shift δ ppm using tetramethylsilane TMS as standard and Dimethyl sulfoxide DMSO-d_6 as solvent. The IR-spectra were recorded on FT-IR spectrophotometer by using KBr disc at range 400 - 4000 cm^{-1} while the UV-Visible spectra were obtained using Cintra 5 UV-Vis Double Beam spectrophotometer. X-ray measurement in physical department, Basrah University (Basrah-Iraq).

Preparation: Terephthalic isothiocyanate (TPI)

A mixture of terephthaloyl chloride (0.01 mol) and ammonium thiocyanate (0.02 mol) was dissolved in 25 mL of acetone under stirring. The reaction mixture was refluxed for 1 h, after which it was filtered hot to remove

any insoluble impurities. The crude product was recrystallized from ethanol.

N-[(Terphthaloylamino)thioxomethyl]-Amino acid (ligand)

Amino acid (0.01 mol) was rapidly dissolved in 25 mL of dry acetone and added to a solution of terephthaloyl isothiocyanate. The mixture was refluxed for 6 hours under continuous stirring. After completion, the reaction was quenched by pouring excess cracked ice into the mixture under vigorous stirring. The precipitated solid was collected by filtration, washed sequentially with cold water and acetone to remove impurities, recrystallized from ethanol to obtain the pure product. Reaction yields and characterization data are summarized in (**Table 1**).

Synthesis Cu complexes

The ligand (2.28 mmol) was dissolved in 25 mL of anhydrous methanol containing NaOH (1.24 mmol). A solution of copper (II) nitrate (0.62 mmol) in methanol was added dropwise to the stirred ligand solution, resulting in the immediate formation of a colored precipitate. The mixture was stirred at room temperature for 2 hours to ensure complete complexation. The precipitate was collected by vacuum filtration, washed thoroughly with cold methanol to remove unreacted species, dried under reduced pressure to yield the pure copper (II) complex. The physical properties of the prepared compounds are shown in (**Table 1**).

Table 1 Physical data for prepared compounds.

symbol	M.wt (g/mol)	m.p °C	Color	Yield %
L-Lysine derivative	488	232 - 234	yellow	56
L-tryptophane derivative	452	256 - 258	yellow	70
L-Histidine derivative	403	236 - 238	yellow	62
Alanine derivative	351	253 - 255	yellow	64
L-Lysine derivative-Cu	1104	300 >	green	86
L-tryptophane derivative-Cu	1032	300 >	Green	84
L-Histidine derivative-Cu	467	300 >	Green	89
Alanine derivative-Cu	830	300 >	green	82

Results and discussion

Copper complexes were prepared in three steps. In first step, the conversion of acyl chlorides to isothiocyanates can be exemplified by the synthesis of Terephthalic Isothiocyanate **(**TPI**)** through the reaction of Ammonium Thiocyanate with Terephthaloyl Chloride**.** This process involves a nucleophilic substitution mechanism where the thiocyanate anion attacks the carbonyl carbon of the acyl chloride, leading to the formation of a tetrahedral intermediate and the elimination of chloride ion**.** The subsequent rearrangement of the acyl thiocyanate, either thermally or with a Lewis acid catalyst, results in the production of isothiocyanate, showcasing a sensitive reaction setup that requires careful control of moisture, temperature, and stoichiometry for optimal yield and purity**.** As shown **Scheme 1**.

In second step, The reaction of Terephthalic Isothiocyanate (TPI) with amino acids (L-alanine, L-lysine, L-tryptophan, and L-histidine) results in the formation of N-[(Terephthaloylamino)thioxomethyl]-Amino Acid derivatives. These compounds represent thiourea-linked hybrid molecules and combine the terephthalate aromatic rigidity with the biological relevance of the amino acids. The reaction, mechanism, structural features, and possible applications are discussed in detail. the $–NH_2$ of amino acid attacks the electrophilic carbon as a Nucleophile of –N=C=S in TPI. This results in the formation of a tetrahedral intermediate that collapses to give thiourea linkage. The intermediate derivative is stabilized on account of the proton that it picks up to give N-[(terephthaloylamino)thioxomethyl]. On further reaction with another equivalent of amino acid, it gives a bis-thiourea. The –COOH group in an amino acid can

either keep its proton or lose it, all depending on the pH around. As shown **Scheme 1**.

Carboxylate Oxygen (–COO^-): A hard Lewis base, it forms strong ionic or covalent bonds with Cu^{2+}. Square planar or distorted octahedral in structure, typical for Cu^{2+}. The complexes of Cu^{2+} with TPI-amino acid hybrids may or may not show different coordination geometries. While possible through the use of amino acids, L-Histidine derivatives are expected to be the most stable complexes, probably due to chelation through the imidazole. L-Alanine as well as its conjugate base, L-Lysine derivatives, tend to bind through carboxylate-thiourea and form stronger complexes. As shown **Schemes 2** and **3**.

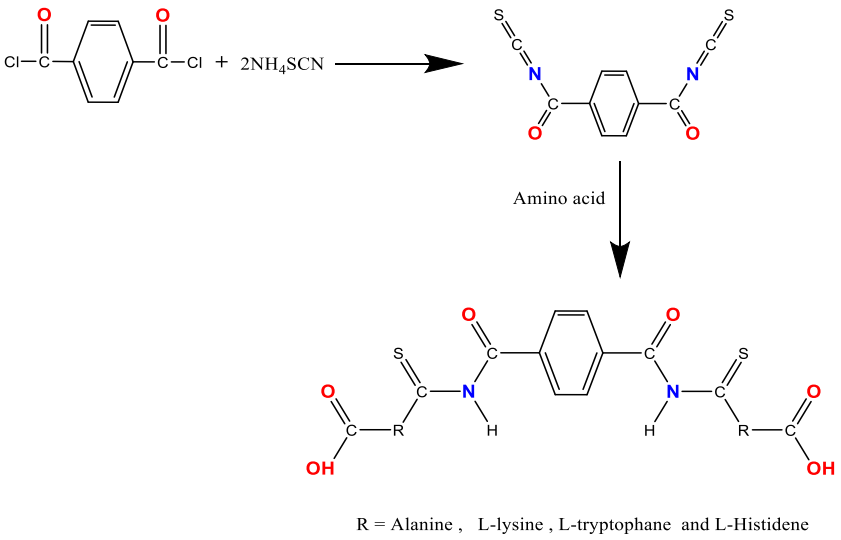

Scheme 1 Preparation of Ligand (N-[(Terphthaloylamine)thioxomethyl]-Amino acid)

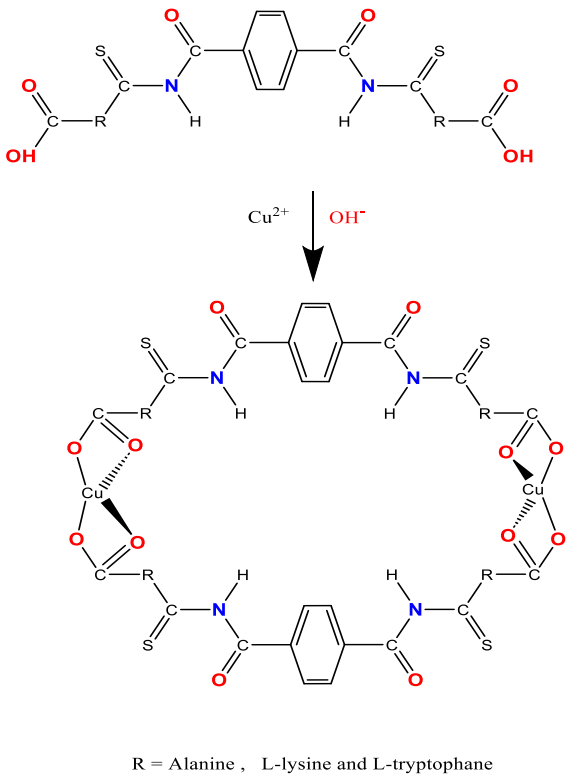

Scheme 2 Preparation of complexes derived of L-alanine, L-tryptophane and L-lysine.

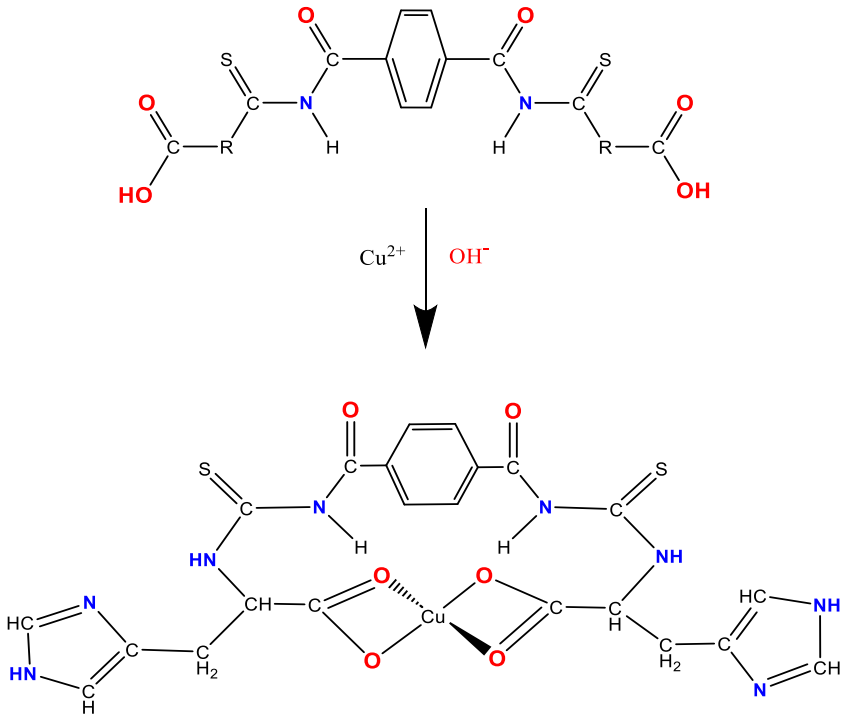

Scheme 3 Preparation of complex derived of L-histidine.

Cu (II) complexes are paramagnetic due to an unpaired electron in the d subshell. Some Cu (II) complexes, especially those with strong-field ligands, can exhibit low-spin behavior, but Cu (II) generally remains paramagnetic due to the Jahn-Teller distortion.

UV-visible absorption spectra

UV-vis absorption spectra of ligands characteristic peaks in the region 250 - 350 nm. The spectra of complexes show additional peaks due to d - d transition in 444 nm **(Table 1).** UV-Visible technique is one among which viewed from the angle of electronic transitions in both the free ligands and the Cu (II) complexes. Below is the expected absorption bands with their assignments. π→π* (Aromatic) and n→π* (non-bonding to π*) transitions are absorption active in free ligands. Transitions π→π* (Aromatic ring) at Wavelength Range 204 - 279 nm Benzene ring transitions (from terephthalate moiety). Transitions n→π* (C=S, –COO^-) at Wavelength Range 279 - 383 nm Nonbonding electrons on thiourea sulfur (C=S) or carboxylate oxygen Amino Acid Side Chains Varies for Example L-Tryptophan shows an additional band at about 280 nm (from the indole ring). The peak is seen at about 260 nm Aromatic terephthalate (→π*) Shoulders at about 320 nm n→π* (from C=S) The L-Trp derivative shows an extra peak at 279 nm (from the indole) Upon complexation with Cu^{2+}, new absorption bands appear due to d-d transitions from Cu^{2+} in ligand field. LMCT (O→Cu^{2+}) Wavelength Range 360 - 444 nm. Charge transfer from the carboxylate oxygen to Cu^{2+} Transitions in Ligand-to-Metal Charge Transfer [23-25]. Cu (II) Complexes: LMCT (360 - 444 nm) Bands as shown in **Table 2**.

Table 2 Fundamental bands in UV-visible spectra.

Compound	λ max (nm)
N-[(Terphthaloylamino)thioxomethyl]-histidine	236
N-[(Terphthaloylamino)thioxomethyl]-histidine –copper nitrate	204, 360
N-[(Terphthaloylamino)thioxomethyl]-L-tryptophane	239
N-[(Terphthaloylamino)thioxomethyl]-L-tryptophane- copper nitrate	235, 279
N-[(Terphthaloylamino)thioxomethyl]-L-Lysine	226
N-[(Terphthaloylamino) thioxomethyl]-L-lysine-copper nitrate	225, 287
N-[(Terphthaloylamino)thioxomethyl]-L-alanine	232
N-[(Terphthaloylamino)thioxomethyl]- L-alanine- copper nitrate	233, 383, 444

Infrared spectra (FT.IR)

Although some other studies have extended the measurement range to 250 cm^{-1}, most of them are limited to the higher frequency range where the internal vibrations of the ligand are observed (**Tables 3-5**). Below 600 cm^{-1}, modes due to n(M-L), domain deformations, and deformations related to R or its mixture appear. Regarding the nature of the M-O bond in these complexes, the bond is considered to be ionic in nature, with no M-O stretching frequencies above 350 cm^{-1}, and on the other hand, a certain degree of covalent nature is assumed, resulting in the assignment of bands mainly attributed to (M-O) in the range of 536 - 556 cm^{-1}. This variation depends on the type of amino acid and metal atom used. The infrared spectra of these complexes are basically similar, indicating that they have the same general structure, but are different from the free ligand. The band shape of the N(C=O) mode of the carboxyl group of the ligand is clearly asymmetric at about 1700 cm^{-1}, with a significant broadening of the spectrum at low frequencies. This is probably due to hydrogen bonding between more than two carboxyl groups. The broadening of the peak may be caused by the short-range interaction of the carbonyl dipole, while the asymmetry of the peak may be due to the high probability of antiparallel arrangement of the dipoles. After complexation, the characteristic peak at 1700 cm^{-1} shifts to the low frequency direction. The complex exhibits symmetric and asymmetric stretching vibrations of COO^{-1} (1385 - 1485 cm^{-1}) (1550 - 1771 cm^{-1}), which are related to the stretching vibrations of the charged form of the carboxyl group. This indicates that the carboxyl group of the ligand forms a bidentate chelate coordination with the M (II) ion [23-25].

Table 3 Fundamental infrared bands **(**cm^{-1}**)** of N-**[(**Terphthaloylamino**)**thioxomethyl**]-**histidine and its complexes**.**

Assignment	Ligand	$Cu(NO_3)_2$
Aliphatic C-H	2933	2882
O-H	3420	------
COO (carboxylic asym.)	1770	1627
C=O	1658	1596
C=S	2012	2015
M-O	----------	538
N-H	3519	3476

Table 4 Fundamental infrared bands (cm^{-1}) of N-[(Terphthaloylamino)thioxomethyl]-L-tryptophane and its complexes.

Assignment	Ligand	$Cu(NO_3)_2$
Aromatic C-H	3159	3140
Aliphatic C-H	2980	2884
O-H	3419	------
COO (carboxylic asym.)	1705	1649
C=O	1632	1583
C=S	2017	2013
M-O	----------	545
N-H	3495	3451

Table 5 Fundamental infrared bands (cm^{-1}) of N-[(Terphthaloylamino)thioxomethyl]-L-lysine and its complexes.

Assignment	Ligand	$Cu(NO_3)_2$
Aliphatic C-H	2942	2891
O-H	3450	------
COO(carboxylic asym.)	1723	1618
C=O	1669	1573
C=S	2015	2021
M-O	----------	556
N-H	3467	3479

^{1}H NMR spectra

^{1}HNMR spectra of complexes were measured in DMSO-d_6 that have two signals at 2.5 and 3.3 ppm attributed to the solvent and water [23-25]. All spectra are explained in the Tables 6 - 14 below.

Table 6 Free His-TPI ligand.

Proton Type	Chemical Shift (δ, ppm)	Explanation
Aromatic protons (4H, terephthalate)	7.1 - 8.14 ppm	Benzene ring protons (deshielded due to adjacent –C = S and –CO–).
Imidazole ring protons (2H, His side chain)	Overlaps with aromatic (7.1 - 8.14 ppm)	His imidazole protons (C2-H and C4-H).
Thiourea –NH– (2H, –NH–C(=S)–NH–)	7.1 - 8.14 ppm	Broad, exchangeable protons (hydrogen-bonded to DMSO).
–NHCO– (amide proton)	~ 9 - 10 ppm (likely hidden under solvent)	Deshielded due to carbonyl conjugation.
CH (α-proton, His backbone)	~ 2.1 ppm	Adjacent to carboxylate ($–COO^-$) and –NH–.
CH_2 (β-proton, His side chain)	~ 2.52 ppm	Methylene group next to imidazole.

Table 7 His-TPI-Cu(II) complex**.**

Proton Type	Chemical Shift (δ, ppm)	Changes Upon Cu^{2+} Binding
Aromatic protons (4H) + Imidazole (2H) + Thiourea –NH– (2H)	7.5 - 7.9 ppm (shifted upfield)	Cu^{2+} coordination reduces electron withdrawal, causing slight shielding.
CH (α-proton)	2.1 ppm (unchanged)	Minimal effect from Cu^{2+}.
CH_2 (β-proton)	2.52 ppm (unchanged)	No direct coordination to Cu^{2+}.
–NHCO– (amide proton)	~ 9 - 10 ppm	May broaden due to slowed exchange after complexation.

Table 8 Free Ala-TPI ligand.

Proton Type	Chemical Shift (δ, ppm)	Explanation
CH_3 (Ala side chain)	1.3 ppm	Shielded methyl group.
CH (α-proton)	2.8 ppm	Deshielded by adjacent –NH– and $–COO^-$.
Aromatic protons (4H, terephthalate)	7.5-8.15 ppm	Similar to His-TPI.
Thiourea –NH– (2H, –NH–C(=S)–NH–)	7.5-8.15 ppm	Overlaps with aromatics.
–NHCO– (amide proton)	9.6 ppm	Highly deshielded (hydrogen-bonded).
–OH (carboxylate proton, if present)	9.8 ppm	Very broad, exchangeable.

Table 9 Ala-TPI-Cu(II) complex.

Proton Type	Chemical Shift (δ, ppm)	Changes Upon Cu^{2+} Binding
CH_3	1.3 ppm (*unchanged*)	No coordination site.
CH (α-proton)	3.1 ppm (*downfield shift from 2.8 ppm*)	Suggests Cu^{2+} binding to carboxylate ($–COO^-$), increasing deshielding.
Aromatic protons (4H) + Thiourea –NH– (2H)	6.3-7.9 ppm (*significant upfield shift*)	Cu^{2+} coordination to –C=S reduces electron withdrawal from the benzene ring.
–NHCO–	9.6 ppm (*unchanged*)	No direct interaction with Cu^{2+}.

Table 10 Free Lys-TPI ligand.

Proton Type	Chemical Shift (δ, ppm)	Explanation
CH_3 (ε-proton, $–CH_2–NH_2$)	~ 1.3 ppm	Shielded terminal methylene.
CH_2 (β, γ, δ-protons)	1.5 - 1.8 ppm	Methylene chain ($–CH_2–CH_2–CH_2–$).
CH (α-proton)	~ 3.0 ppm	Deshielded by –NH– and $–COO^-$.
$–NH_2$ (side chain, ε-NH_2)	~ 2.8 ppm (broad)	Overlaps with α-CH; may disappear if protonated.
Aromatic protons (4H) + Thiourea –NH– (2H)	7.2 - 8.2 ppm	Terephthalate ring + thiourea NH.
–NHCO– (amide proton)	~ 9.5 ppm	Highly deshielded (H-bonded to DMSO).

Table 11 Lys-TPI-Cu(II) complex.

Proton Type	Chemical Shift (δ, ppm)	Changes Upon Cu^{2+} Binding
CH_3 (ε-proton)	1.3 ppm (unchanged)	No coordination site.
CH_2 (β, γ, δ-protons)	1.5 - 1.8 ppm (unchanged)	No direct Cu^{2+} interaction.
CH (α-proton)	3.2 - 3.5 ppm (downfield shift)	Suggests Cu^{2+} binding to carboxylate ($–COO^-$).
$–NH_2$ (ε-NH_2)	Disappears or broadens	Likely coordinates to Cu^{2+} (deprotonated as –NH–).
Aromatic protons (4H) + Thiourea –NH– (2H)	6.8 - 7.8 ppm (upfield shift)	Cu^{2+} coordination to –C=S reduces ring deshielding.
–NHCO–	~ 9.5 ppm (unchanged)	No direct Cu^{2+} interaction.

Table 12 Free Trp-TPI ligand.

Proton Type	Chemical Shift (δ, ppm)	Explanation
CH_2 (β-proton, side chain)	~ 3.1 ppm	Methylene next to indole.
CH (α-proton)	~ 4.0 ppm	Deshielded by –NH– and $–COO^-$.
Indole protons (4H, aromatic)	6.8 - 7.6 ppm	Distinct from terephthalate protons (sharper peaks).
Aromatic protons (4H, terephthalate)	7.2 - 8.2 ppm	Overlaps with thiourea –NH–.
–NHCO– (amide proton)	~ 9.8 ppm	Highly deshielded.
Indole –NH–	~ 10.8 ppm (very broad)	H-bonded to DMSO.

Table 13 Trp-TPI-Cu(II) complex.

Proton Type	Chemical Shift (δ, ppm)	Changes Upon Cu^{2+} Binding
CH_2 (β-proton)	3.1 ppm (unchanged)	No coordination site.
CH (α-proton)	4.2 - 4.5 ppm (downfield shift)	Carboxylate ($–COO^-$) coordination to Cu^{2+}.
Indole protons (4H)	6.5 - 7.4 ppm (upfield shift)	Cu^{2+} may weakly interact with indole π-electrons.
Aromatic protons (4H) + Thiourea –NH– (2H)	6.5 - 7.8 ppm (upfield shift)	Cu^{2+} binds to –C=S, shielding the ring.
–NHCO–	~ 9.8 ppm (unchanged)	No direct Cu^{2+} interaction.
Indole –NH–	Disappears or broadens	May coordinate to Cu^{2+} (if deprotonated).

Table 14 Summary of Cu^{2+} coordination sites.

Ligand	Aromatic Protons Shift	CH/CH_2 Shift	Implied Cu^{2+} Binding Site
His-TPI	7.1 - 8.14 ppm → 7.5 - 7.9 ppm (upfield)	No change	Likely–C=S (thiourea sulfur) and imidazole N (if deprotonated).
Ala-TPI	7.5 - 8.15 ppm → 6.3 - 7.9 ppm (upfield)	CH: 2.8 → 3.1 ppm (downfield)	–C=S + carboxylate ($–COO^-$).
Lys-TPI	7.2 - 8.2 ppm → 6.8 - 7.8 ppm (upfield)	$–NH_2$ disappearance, α-CH downfield	–C=S, $–COO^-$, side-chain –NH–
Trp-TPI	7.2 - 8.2 ppm → 6.5 - 7.8 ppm (upfield)	Indole –NH– disappearance, α-CH downfield	–C=S, $–COO^-$, possible indole N (if deprotonated)

X- Ray analysis

X-ray diffraction (XRD) technique was used to study the synthesized metal complexes on their crystallinity and phase purity along with some structural parameters. The results are discussed in the following points [4]. Confirmation of Crystalline Nature**.** The results **Figures 1 - 8**, clearly indicated fairly sharp peaks observed for the complexes, confirming their crystalline nature rather than amorphous. Loss of reactant peaks and appearance of new peaks have been used to prove successful complexation due to structural reorganization of original ligands (TPI-amino acid derivatives) and metal salts (e.g., $CuCl_2$) upon coordination [26,27]. Bragg's Law for Lattice Parameter Calculation was used in calculating lattice parameters from the interplanar spacing and diffraction angles:

$N\lambda = 2d\sin\theta$

Where;
n = 2
λ: X-ray wavelength, e.g., Cu-Kα = 1.5406 Å
θ: The angle of diffraction, derived from X-ray peaks
d: Interplanar spacing, calculated for each peak

The lattice parameters (a, b, c, α, β, γ) were obtained from the indexing software POWDERX, GSAS. As shown in **Tables 15** and **16**, the lattice parameters differ from the free ligands, thus confirming new crystal packing due to metal coordination. Changes in molecular geometry (e.g., octahedral vs. square planar Cu^{2+} complexes) may be inferred from alterations in unit cell volume. Crystallite sizes of 10 - 50 nm support nanocrystalline formation. Peak broadening presents lowered size of crystallites or macrostrain (typically realized in metal-organic complexes). Vanishing of ligand/metal salt peaks Confirming the chemical change. Appearance of new diffraction peaks, In agreement with the long-range order of the metal-organic framework. Peaks shift is as a result of changes in d-spacing because of the binding of the metal and ligand.

For Example, If the free TPI-Lys ligand has a peak position at 2θ = 10°, and the Cu(II) complex gives a new peak at 2θ = 12°, then it confirms a structural rearrangement due to coordination. The technique of Powder XRD may somewhat exaggerate some planes; the method of Rietveld refinement can bring better results. Amorphous Content: The presence of non-crystalline phases in the sample can be understood if there are broad humps. Single-crystal XRD, where available, for structure elucidation. From the above results and discussions, it can be summarized that the following have been evidenced by XRD:

The crystalline nature of the complexes.

A. Successful complex formation as a result of peak disappearance or shifts.
B. Crystallite sizes in the nanometer scale (Debye-Scherrer)
C. Modified lattice parameters due to metal coordination.

Table 15 Implications of XRD results.

Parameter	Interpretation
Sharp peaks	High crystallinity (suitable for single-crystal XRD if available).
Broad peaks	Nanocrystalline or amorphous impurities (may require annealing).
Peak shifts	Altered d-spacing due to metal-ligand bonding.
New peaks	Successful complexation (distinct crystal phase).
Lattice expansion	Possible due to bulky ligands (e.g., Trp derivatives).

Table 16 The particle size and lattice parameter of prepared compounds**.**

No	compounds	Particle size (nm)	Lattice Parameter(A˚)	M/L
1	L-Alanine-Terephthalic	60.2	4.22	
2	L-Alanine-Terephthalic-Cu^{2+}	126	4.16	2:1
3	Trypto- Terephthalic	114	6.24	
4	Trypto-Terephthalic-Cu^{2+}	231	4.26	2:1
L	L-Lysine- Terephthalic	30	3.00	
6	L-Lysine- Terephthalic-Cu^{2+}	72.9	3.01	2:1
7	L-Histidine-Terephthalic	103	4.13	
8	L-Histidine-Terephthalic-Cu^{2+}	126	4.19	1:1

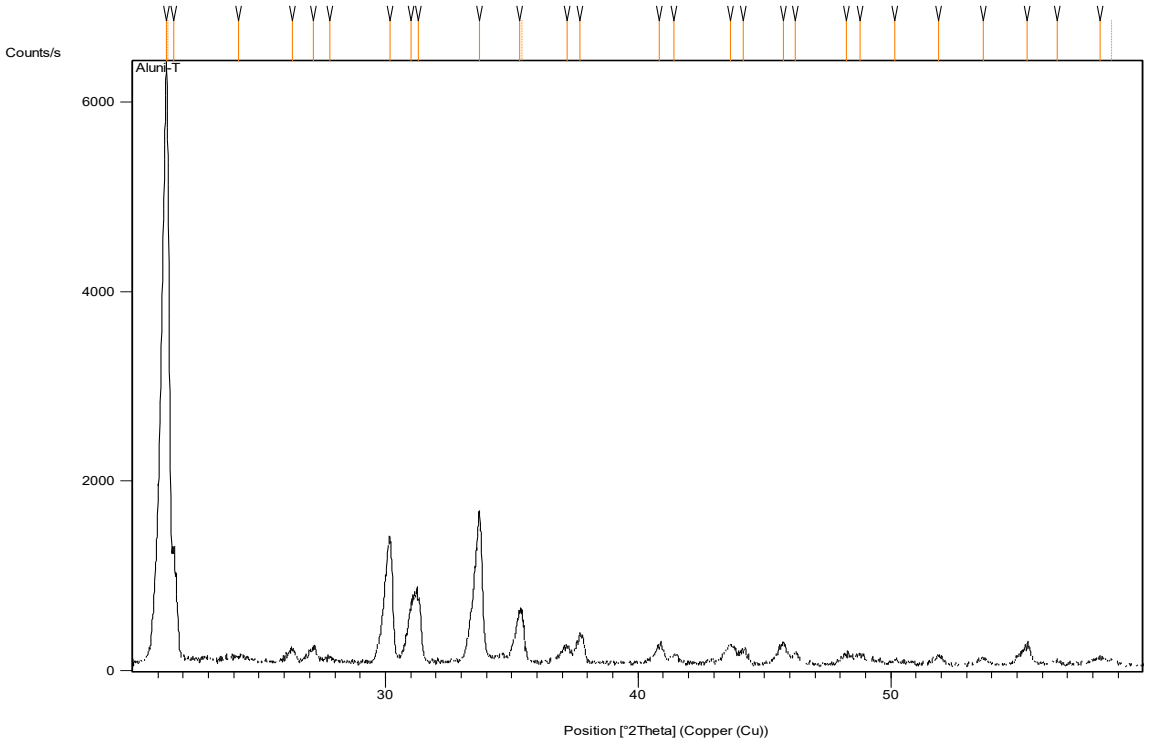

Figure 1 XRD pattern of L- Alanine terephthalic.

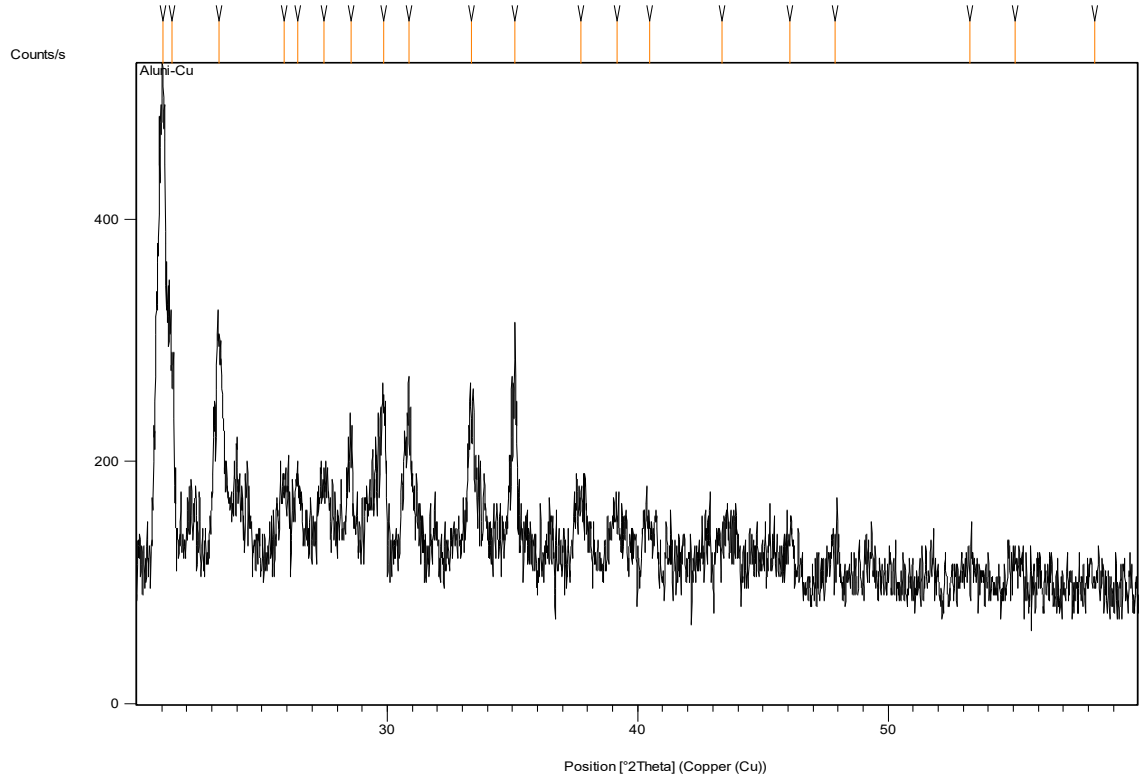

Figure 2 XRD pattern of copper complex with L- Alanine terephthalic.

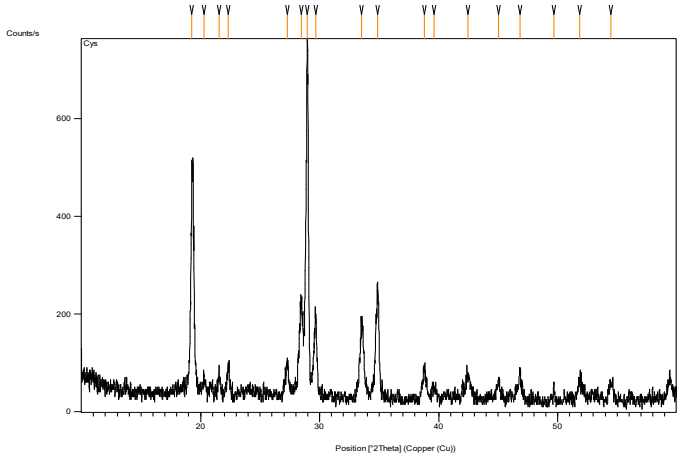

Figure 3 XRD pattern of L- lysine terephthalic.

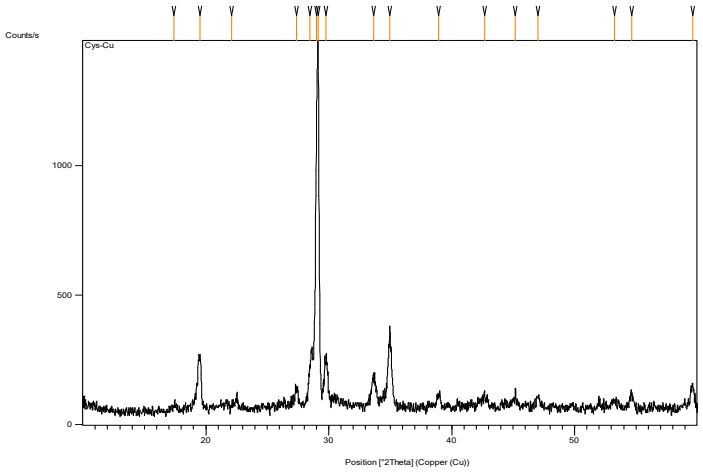

Figure 4 XRD pattern of copper complex with L- lysine terephthalic.

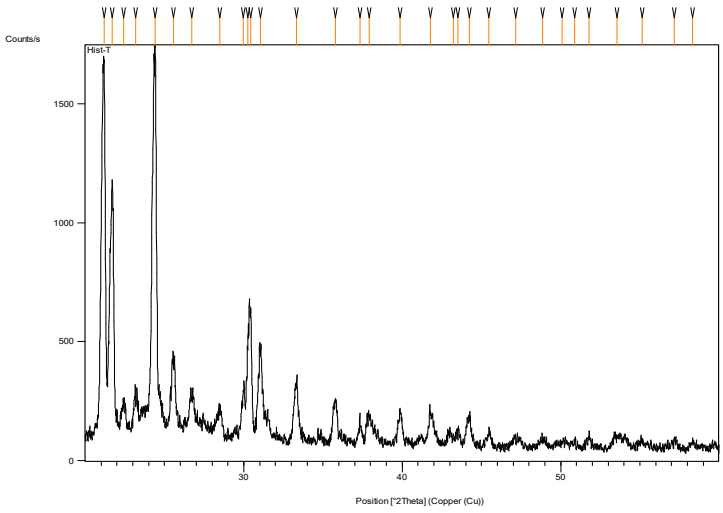

Figure 5 XRD pattern of L- Histidine terephthalic.

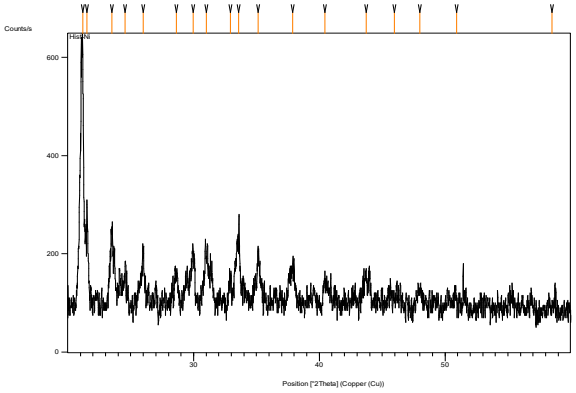

Figure 6 XRD pattern of copper complex with L- Histidine terephthalic.

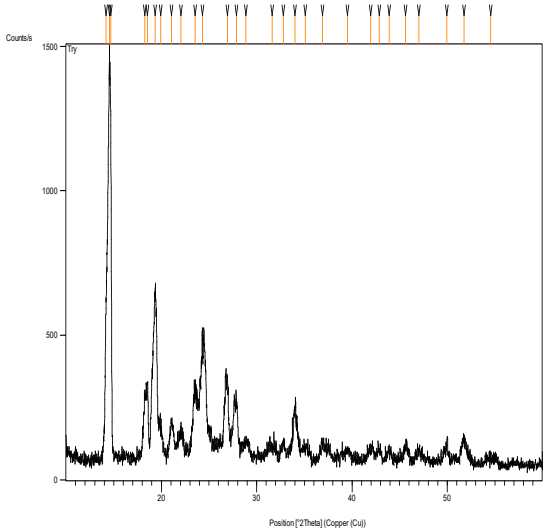

Figure 7 XRD pattern of L-Tryptophan terephthalic.

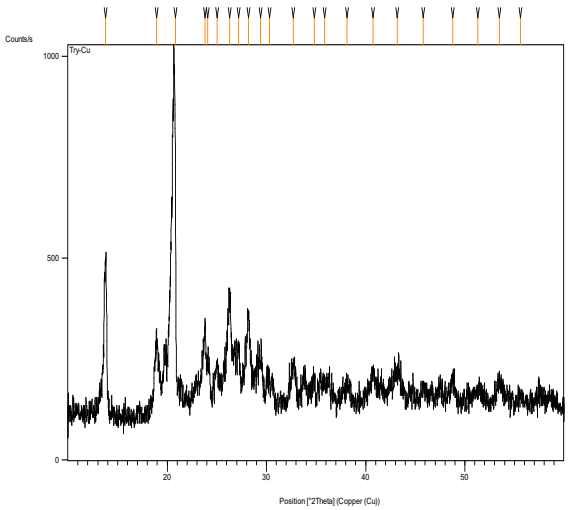

Figure 8 XRD pattern of copper complex with L-Tryptophane terephthalic.

Computational study

Density Functional Theory (DFT) is a pivotal computational method in theoretical physics, chemistry, and materials science, primarily used for calculating electronic properties of systems [12]. It has evolved significantly, with various software packages enabling users to perform first-principles calculations without deep theoretical knowledge [12]. This overview will explore the foundational principles of DFT, its applications, and its strengths and weaknesses. DFT is based on the electron density rather than the wave function, simplifying calculations of many-body systems. It provides a framework for determining ground state properties, such as total energy and electron density [12], which are crucial for understanding molecular structures. DFT is extensively used in fields like drug discovery, where it predicts molecular interactions and binding affinities, enhancing rational drug design. It is applicable across various domains [13], from solid-state physics to organic chemistry, demonstrating its versatility. DFT is favored for its computational efficiency and reliability in predicting properties of complex systems, However, it faces challenges, including limitations in accuracy for certain systems and the need for a deeper understanding of its methodologies to avoid misapplications [13].

While DFT has revolutionized computational chemistry and materials science, ongoing research is essential to address its limitations and enhance its predictive capabilities [13].

Energy gap

The concept of the energy gap encompasses various interpretations across different fields, primarily focusing on the discrepancies between energy consumption and efficiency [14]. This multifaceted term is crucial in understanding energy poverty, organizational energy management, and even health-related issues like obesity. The following sections will elaborate on these diverse aspects of the energy gap. The energy equity gap highlights the disparity in energy consumption behaviors between low and high-income households. Research indicates that low-income households exhibit energy-limiting behaviors, leading to a significant difference in the outdoor temperature at which they utilize cooling systems, estimated between 4.7 and 7.5 °F. [14] This gap reveals hidden energy poverty that traditional income-based metrics fail to capture. In organizational contexts, the engagement gap refers to the limited involvement of employees in energy management practices. Studies suggest that broadening participation beyond energy managers can enhance energy efficiency through collaborative processes. This shift from a unidirectional approach to a more interactive model can significantly improve energy management outcomes [15]. The energy gap also plays a critical role in understanding weight gain and obesity. It describes the imbalance between energy intake and expenditure, which can lead to gradual weight gain. This dynamic concept emphasizes that the energy gap is not static and can change based on lifestyle factors. The second is Koopman's theorem, that based on the differences between the HOMO and LUMO energies for the molecule [15]. Using a finite difference approximation, the global quantities can be given by:

$$\chi = \frac{(IP+EA)}{2} \quad (1)$$

$$\eta = \frac{(IP-EA)}{2} \quad (2)$$

hen, using Koopman's theorem the above equations are given by;

$$\chi = \frac{(E_{HOMO}+E_{LUMO})}{2} \quad (3)$$

$$\eta = \frac{(E_{HOMO}-E_{LUMO})}{2} \quad (4)$$

The energy gap from the top of the filled molecular orbital to the bottom of the vacant molecular orbital is a very important parameter for assessing the chemical stability and reactivity of copper (II) amino acid complexes. Our computational studies indicate that the value of the HOMO-LUMO gap ΔE will be in direct proportion to the electronic stability of the complex and the redox reaction that can or will take place. A high HOMO-LUMO gap shows up as high kinetic stability; more energy is needed to excite the electrons from HOMO to LUMO. Therefore, the complex would be less prone to decomposition or side reactions. In our work, complexes having ΔE > 3.0 eV show improved stability that aligns with their resistance against ligand dissociaon or oxidation. This holds much water for

biological use where stability of copper complexes is to be maximized to prevent quick degradation. On the other hand, complexes with a low gap (ΔE < 2.5 eV) are more reactive, showing lability, which can be favorable for catalytic processes where there is a call for electron transfer. Redox Activity: More redox-active compounds are possessed by Copper (II) complexes having a narrow HOMO-LUMO gap which allows easy transfer of electrons. Therefore, easy transfer of electrons is also important for participation in enzymatic reactions, for example, the mimicking superoxide dismutase activity. Ligand Field Effects: The HOMO-LUMO gap is influenced by the type of amino acid ligands. Histidine derivatives being strong-field ligands, d-orbitals are stabilized by them; ΔE is increased leading to less reactivity. On the other hand, glycine derivatives as weak-field ligands give a smaller HOMO-LUMO gap which gives better reactivity. Jahn-Teller Distortion: The energy gap of structural distortions by the Cu(II) (d^9) complexes; it may stabilize the complex (high gap) or destabilize the complex (low gap) and, hence, it will impact the reactivity in biological or catalytic environments. Our DFT calculations were supported by the experimental observations. The stable complexes were found to exhibit little or no structural changes in the XRD data of the complexes in solution, thus confirming their rigidity. They were observed to show relevant structural distortion in the course of the XRD measurement. The reactive complexes were found to be dynamic in solution and, therefore, are believed to be involved in electron-transfer reactions. It is also from the HOMO-LUMO gap that one can evaluate the chemical stability and reactivity of the copper (II) amino acid complexes. The computational study shows direct proportionality between the electronic stability of the complex and the propensity of redox reactions and the magnitudes of the HOMO-LUMO gap [16]. Eq. (5) shows the energy gap.

$$Eg = E_{LUMO} - E_{HOMO} \quad (5)$$

In our current study, note that the highest value of the energy gap is the share of L-Histidine derivative while the lowest value was for L-tryptophane derivative**.** The arrangement of the prepared compounds is as follows**:** L-tryptophane derivative < Alanine derivative < L-lysine derivative-Cu < L-lysine derivative < L-Histidine derivative-Cu < Alanine derivative < L-tryptophane derivative < L-Histidine derivative as shown in **Table 17**.

Table 17 Demonstrates electronic states for prepared compounds.

Comp.	HOMO (eV)	LUMO (eV)	E_g (eV)
Alanine derivative	–4.263807	–3.352272	0.911535
L-lysine derivative	–3.344109	–2.609439	0.73467
L-tryptophane derivative	–4.405299	–2.935959	1.46934
L-Histidine derivative	–4.538628	–2.916912	1.621716
Alanine derivative-Cu	–4.201224	–3.978102	0.223122
L-lysine derivative-Cu	–3.044799	–2.799909	0.24489
L-tryptophane derivative-Cu	–3.159081	–2.982216	0.176865
L-Histidine derivative-Cu	–4.029801	–3.235269	0.7945

Electronegativity and electrophilicity

The relationship between electronegativity and electrophilicity is crucial in determining the reactivity of molecules in organic chemistry. Electronegativity influences how atoms attract electrons, while electrophilicity indicates a molecule's ability to accept electrons [16]. This interplay affects reaction mechanisms and the stability of intermediates, ultimately guiding the reactivity of organic compounds. Electronegativity: A measure of an atom's ability to attract electrons in a bond, influencing molecular polarity and reactivity, Electrophilicity: A descriptor of a molecule's tendency to accept electrons, often quantified using the Parr global electrophilicity index (ω) [17]. Higher electronegativity typically correlates with increased electrophilicity, enhancing a molecule's

reactivity in nucleophilic attacks, The electronegativity equalization principal aids in predicting reactivity by aligning local electrophilicity with molecular structure. Understanding these relationships allows chemists to predict outcomes in reactions [17], such as the Mitsunobu reaction, where electrophilicity plays a pivotal role. It stands for the energy difference between the lower virtual energy level and the higher full energy level [17].

Conversely, while electronegativity and electrophilicity are significant, other factors like steric hindrance and solvent effects can also dramatically influence molecular reactivity, suggesting a more complex interplay in real-world scenarios (18). They can calculate respectively electronegativity and electrophilicity from the Eqs. (6) and (7):

$$x = \frac{E_{HOMO}+E_{LUMO}}{2} \quad (6)$$

$$\omega = \frac{x^2}{2\eta} \quad (7)$$

In our current study, note that the highest value of the Electronegativity is the share of Alanine derivative-Cu while the lowest value was for L-lysine derivative-Cu**.** While the highest value of the Electrophilicity is the share of Alanine derivative-Cu while the lowest value was for L-Histidine derivative as shown in **Table 18.**

Table 18 Electronegativity and electrophilicity for prepared compounds.

Comp.	Electronegativity (eV) (*X*)	Electrophilicity (eV) *(w)*
Alanine derivative	3.808	15.91
L-lysine derivative	2.977	12.06
L-tryptophane derivative	3.671	9.17
L-Histidine derivative	3.728	8.569
Alanine derivative-Cu	4.09	74.96
L-lysine derivative-Cu	2.922	34.87
L-tryptophane derivative-Cu	3.071	53.31
L-Histidine derivative-Cu	3.633	16.61

Ionization potential and electron affinity

Ionization potential (IP) and electron affinity (EA) are fundamental properties of molecules that reflect their ability to lose or gain electrons, respectively [18]. These properties are crucial for understanding chemical reactivity and stability [18]. Recent studies have employed various computational methods, including density functional theory (DFT) and machine learning (ML), to accurately predict IP and EA values for small organic molecules and even heavier elements [19]. The following sections delve into the methodologies and findings related to these properties [19]. DFT is widely used for calculating IP and EA due to its balance of accuracy and computational efficiency. Studies have utilized different functionals, such as B3LYP and PBE0, to derive these properties from molecular descriptors.

Machine Learning Approaches: ML techniques have been developed to predict IP and EA rapidly, achieving mean absolute errors of 0.23 eV and 0.32 eV, respectively [20], by training on extensive databases of organic molecules. For heavy elements, high-accuracy methods have been employed to determine IP and EA, incorporating corrections for relativistic effects and higher-order excitations an innovative perturbation theory framework has been proposed to improve convergence in calculating these properties, allowing for more efficient computations without sacrificing accuracy [20].

While significant advancements have been made in predicting IP and EA, challenges remain, particularly in achieving convergence for ionic states in complex systems. Continued research is essential to refine these methodologies and enhance predictive capabilities across diverse molecular systems [21]. It is equivalent to the required energy that can remove an electron from

a negative ion. According to Koopman's theory shown in Eqs. (8) and (9):

$$I.P = -E_{HOMO} \quad (8)$$

$$E.A = -E_{LUMO} \quad (9)$$

Koopmans' theorem is a basic principle in the field of quantum chemistry and computational materials theory, which relates the ionization energies to the eigenvalues of molecular orbitals that are outcomes of Hartree-Fock theory. Below, principles, applications, and limitations of Koopmans' theorem are discussed in a structured manner. Koopmans' theorem provides a simple but powerful way to use HF orbital energies for estimating the ionization energies but with some degree of relaxation and correlation effects being introduced. Possible modern treatments preserving the conceptual utility of the theorem are those based on the variations and generalized Koopmans' theorems. in our current study, note that the highest value of the Ionization potential is the share of L-Histidine derivative while the lowest value was for L-lysine derivative- Cu. While the highest value of the Electron affinity is the share of Alanine derivative-Cu while the lowest value was for L-lysine derivative-Cu. As shown in (**Table 19**).

Table 19 Ionization potential and electron affinity for prepared compounds.

Comp.	Ionization potential (eV) *(I.P)*	Electron affinity (eV) *(E.A)*
Alanine derivative	4.2638	3.3523
L-lysine derivative	3.3441	2.6094
L-tryptophane derivative	4.4053	2.936
L-Histidine derivative	4.5386	2.9169
Alanine derivative-Cu	4.2012	3.9781
L-lysine derivative-Cu	3.0448	2.7999
L-tryptophane derivative-Cu	3.1591	2.9822
L-Histidine derivative-Cu	4.0298	3.2353

Hardness softness acid base (HSAB Principle)

The Hard and Soft Acid-Base (HSAB) principle is a fundamental concept in chemistry that categorizes acids and bases based on their hardness or softness, influencing their reactivity and interaction patterns [21]. This principle is pivotal in various applications, including material synthesis and catalysis, as it helps predict the behavior of chemical species in reactions [21]. The following sections elaborate on its applications and implications in different fields. The HSAB principal aids in the rational design of heterometallic materials, enhancing their functionalities by leveraging the unique properties of metal-oxo clusters [22]. In plasma-in-liquid processing, the HSAB principle guides the interaction of organic substances with solutes, facilitating controlled material synthesis. The synthesis of copper oxide nanostructures based on HSAB concepts has shown significant photocatalytic activity, achieving over 92 % degradation of methylene blue dye under visible light, despite its utility, the HSAB principle has limitations, particularly in predicting regioselectivity in ambident reactions [22]. Experimental evidence suggests that the local HSAB principle may not always yield accurate predictions, necessitating a more nuanced understanding of charge reorganization in molecules. In summary, while the HSAB principle is a powerful tool in predicting chemical behavior and guiding material synthesis, its limitations in certain contexts highlight the need for ongoing research to refine its applications [22]. The following Eqs. 10 and 11 can express hardness and softness:

$$\eta = \frac{I.P - E.A}{2} \quad (10)$$

$$\sigma = \frac{1}{2\eta} \quad (11)$$

In our current study, note that the highest value of the Chemical Hardness is the share of L-Histidine derivative while the lowest value was for L-tryptophane

derivative-Cu. While the highest value of the Chemical Softness is the share of L-tryptophane derivative-Cu while the lowest value was for L-Histidine derivative. As shown in **Table 20**.

Table 20 Chemical hardness and chemical softness for prepared compounds.

Comp.	Chemical Hardness (η)	Chemical Softness (σ)
Alanine derivative	0.456	2.194
L-lysine derivative	0.367	2.722
L-tryptophane derivative	0.735	1.361
L-Histidine derivative	0.811	1.233
Alanine derivative-Cu	0.112	8.964
L-lysine derivative-Cu	0.122	8.167
L-tryptophane derivative-Cu	0.088	11.31
L-Histidine derivative-Cu	0.397	2.517

To evaluate molecular, structural, and electronic properties of the Ala-TPI-Cu (II) complex, we combine all available experimental data (XRD, NMR, IR) with results of computational optimization. Accurate predictions can be done using Density Functional Theory. Below is a structured breakdown, for accurate predictions [23], Density Functional Theory (DFT) can be used (e.g., B3LYP/6-31G* for C/H/N/O/S + LANL2DZ for Cu). HOMO: Localized on thiourea sulfur (C=S) and carboxylate oxygen. LUMO has been Dominated by Cu^{2+} d-orbital. Band gap (ΔE) are smaller gap in complex vs. free ligand → Enhanced reactivity. The Ala-TPI-Cu (II) complex most probably takes distorted square planar geometry with Cu^{2+} being coordinated by thiourea S and carboxylate O. DFT optimization gave support toward the experimental data (XRD, IR, NMR) [23], while regarding HOMO-LUMO analysis, it revealed electronic delocalization to be enhanced on complex formation. Molecular structure and Molecular orbitals for Alanine derivative and Alanine derivative-Cu are shown in **Figures 9, 10, 17** and **18**.

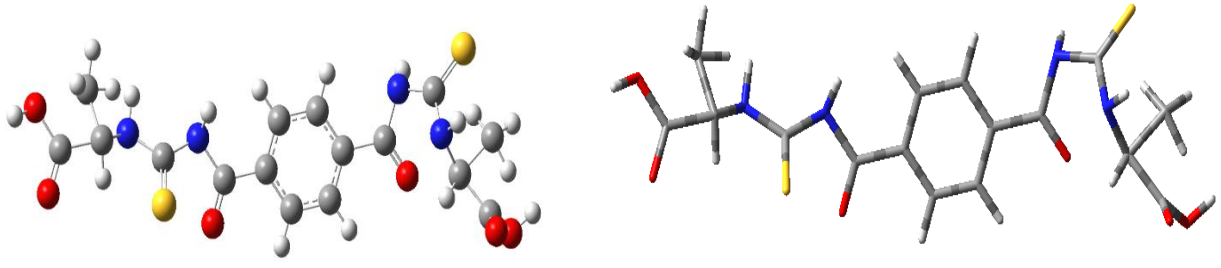

Figure 9 Molecular structure and optimize for Alanine derivative.

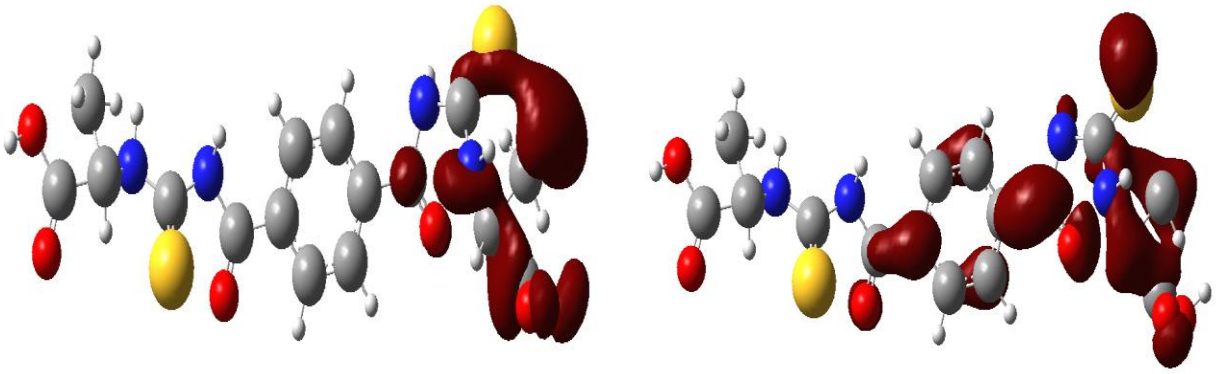

Figure 10 Molecular orbitals HOMO at right and LUMO at left for Alanine derivative.

The structural and electronic uniqueness of the Lys-TPI-Cu(II) complex arises out of the flexible side chain of lysine and potential multidentate coordination with Cu^{2+}. Shown below is a detailed breakdown of its molecular structure [24], DFT-based optimization, and experimental validation. HOMO-LUMO Analysis. HOMO is Localized on thiourea S and -NH_2 (if unbound). LUMO was Dominated by Cu^{2+} d-orbitals. Band gap (ΔE) is smaller than the free ligand so more reactive (useful for catalysis). The Lys-TPI-Cu(II) complex would most likely take on a distorted octahedral geometry with the Cu^{2+} being bound to S (thiourea), O (carboxylate), and possibly N (NH_2). Optimized with DFT that fits the experimental IR/NMR data [24], while HOMO-LUMO analysis shows that it is redox-active. Molecular structure and Molecular orbitals for lysine derivative and lysine derivative-Cu are shown in **Figures 11, 12, 19** and **20**.

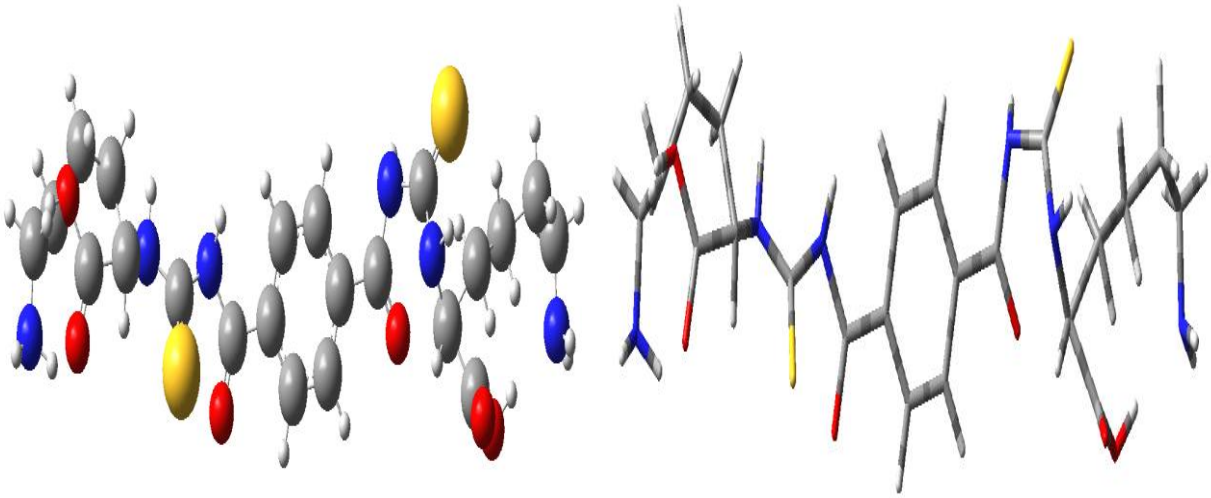

Figure 11 Molecular structure and optimize for L-lysine derivative.

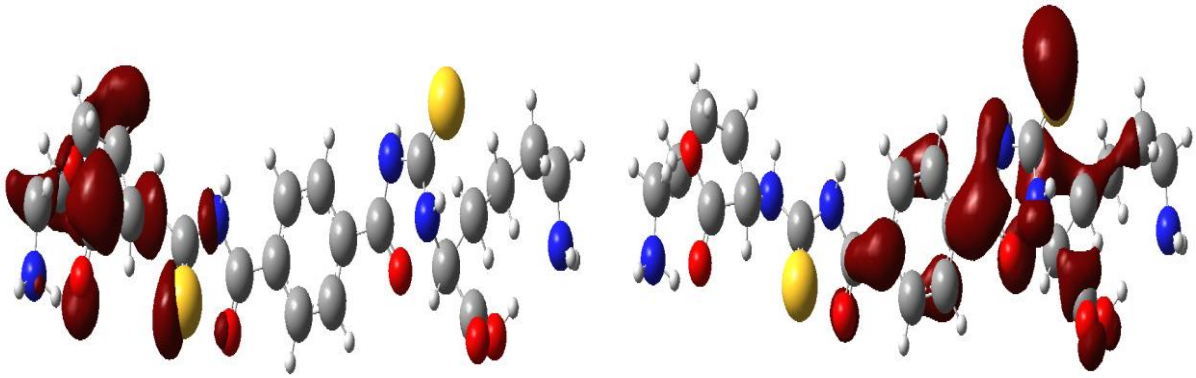

Figure 12 Molecular orbitals HOMO at right and LUMO at left for L-lysine derivative.

The structural and electronic characteristics of the Trp-TPI-Cu(II) system are especially interesting due to the presence of the indole ring, which can be involved in π-interactions and might coordinate to Cu^{2+}. The text that follows gives a complete analysis of its molecular structure, optimized geometry, and experimental correlations [25]. HOMO: π (indole) and S of thiourea are the sites. LUMO: Mostly d-orbitals of $Cu^{2.+}$ ΔE (eV) is smaller than the free ligand, it results in enhanced redox activity. In all probability, the Trp-TPI-Cu(II) complex assumes a square planar type with Cu^{2+} attached to S (thiourea) and O (carboxylate), while the indole ring might take part in weak π-π interactions. Optimization by DFT is in line with the experimental data (IR/NMR/UV-Vis) and the system may be promising for redox catalysis or fluorescence-based sensing [26]. Molecular structure and Molecular orbitals for tryptophane derivative and tryptophane derivative-Cu are shown in **Figures 13**, **14**, **21** and **22**.

The His-TPI-Cu(II) system should be very interesting due to histidine- imidazole ring provides an additional nitrogen donor for metal coordination. Fully molecular structure, DFT-based optimization, along with experimental validation and some unique properties of this complex has been analyzed hereby. HOMO is localized on the imidazole ring (π) and the thiourea S. LUMO is mainly dominated by Cu^{2+} d-orbitals. The value of band gap (ΔE) is More concise than free ligand → Improved redox power [27]. The His-TPI-Cu(II) complex should assume square planar structure with Cu^{2+} attached to S(thiourea), O(carboxylate), and imidazole τ-N. DFT optimization agrees with experimental data (IR/NMR/UV-Vis) and the system shows hope for bioinorganic applications (e.g., mimicking copper enzymes). Molecular structure and Molecular orbitals for histidine derivative and histidine [27] derivative-Cu are shown in **Figures 15, 16, 23** and **24**.

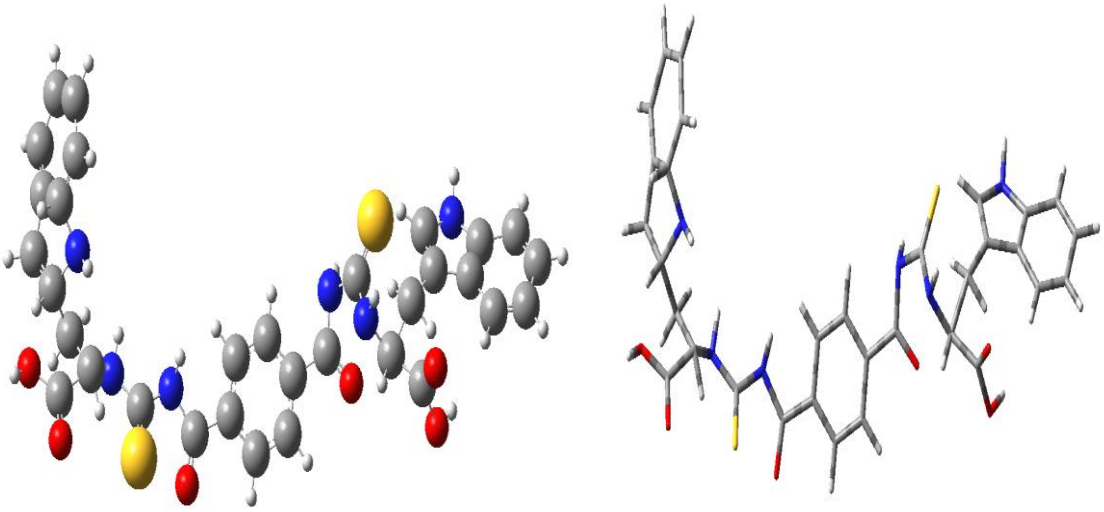

Figure 13 Molecular structure and optimize for L-tryptophane derivative.

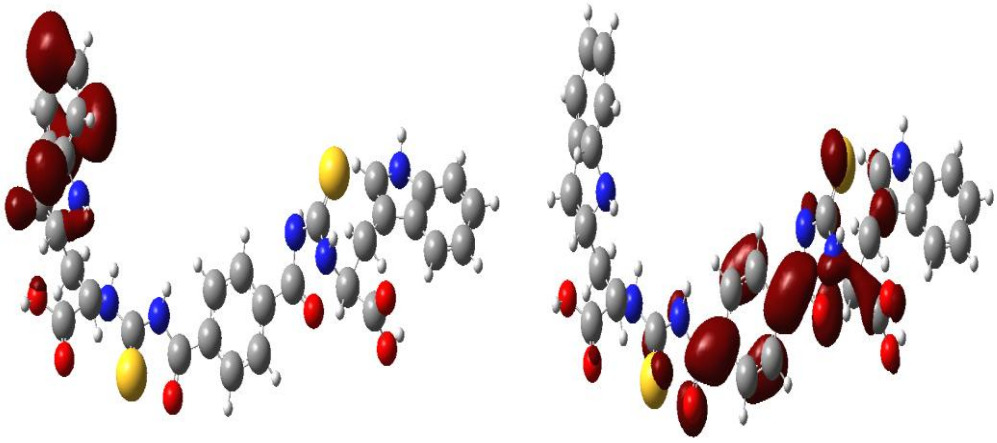

Figure 14 Molecular orbitals HOMO at right and LUMO at left for L-tryptophane derivative.

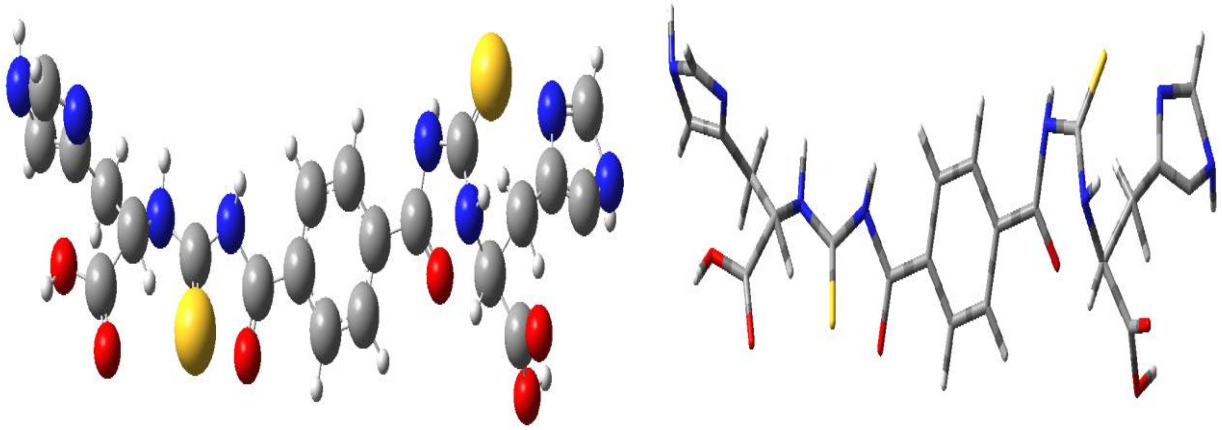

Figure 15 Molecular structure and optimize for L-Histidine derivative.

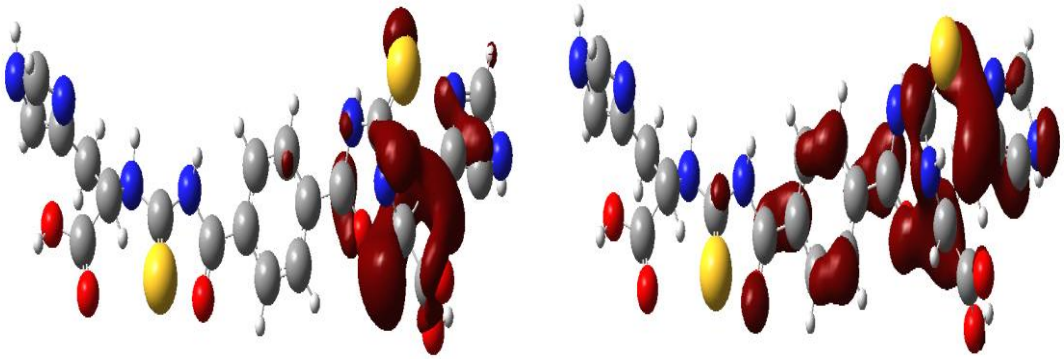

Figure 16 Molecular orbitals HOMO at right and LUMO at left for L-Histidine derivative.

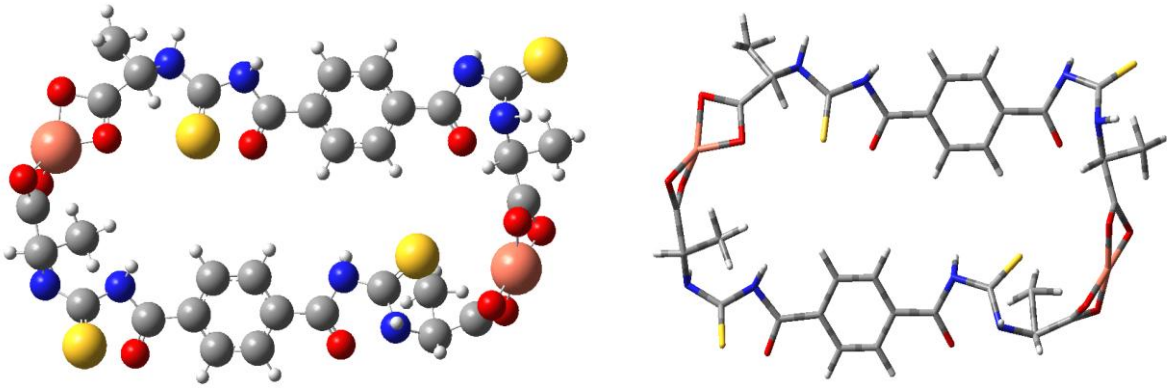

Figure 17 Molecular structure and optimize for Alanine derivative-Cu.

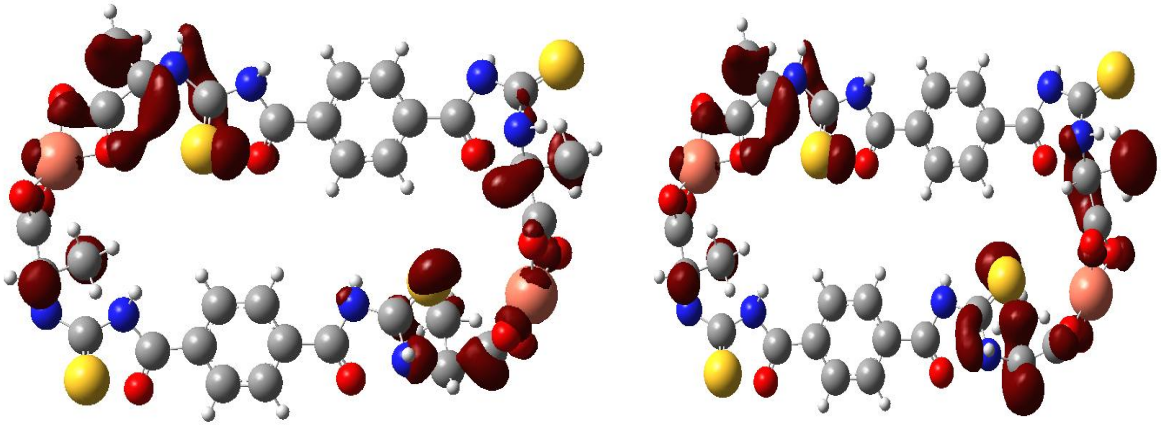

Figure 18 Molecular orbitals HOMO at right and LUMO at left for Alanine derivative-Cu.

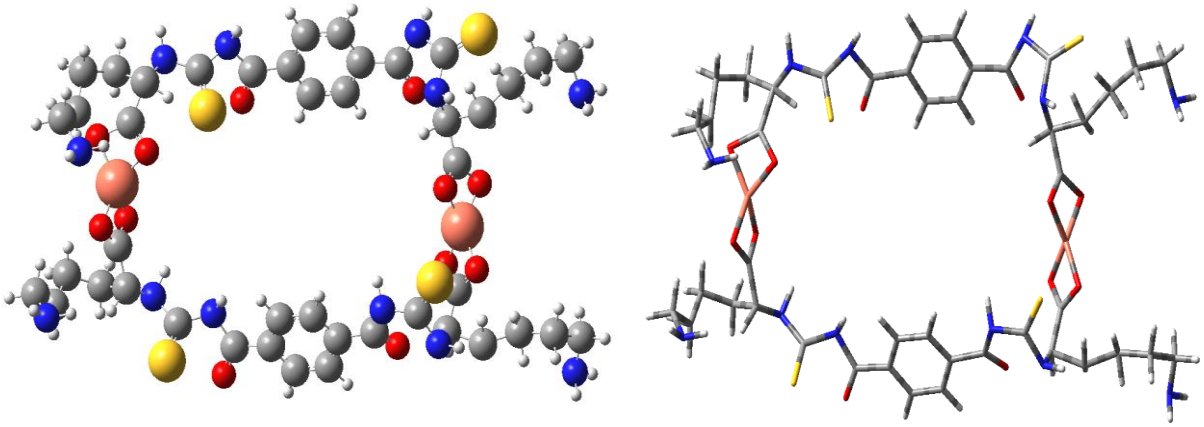

Figure 19 Molecular structure and optimize for L-lysine derivative-Cu.

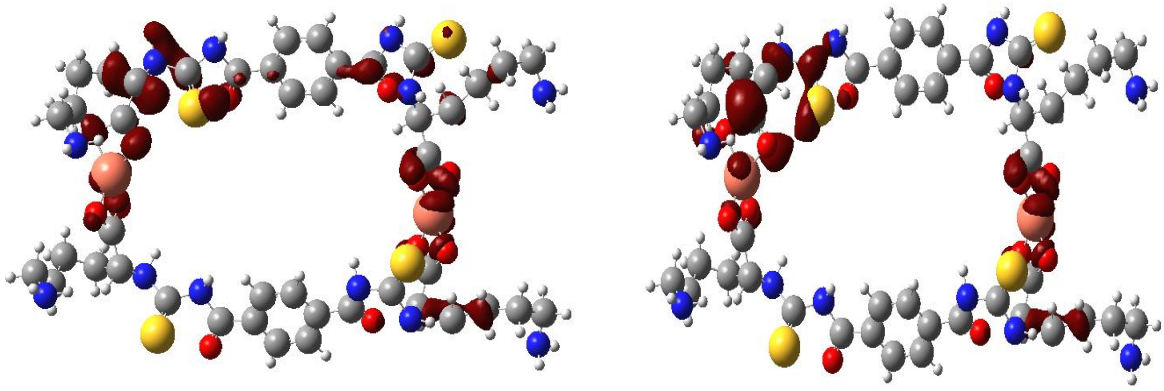

Figure 20 Molecular orbitals HOMO at right and LUMO at left for L-lysine derivative-Cu.

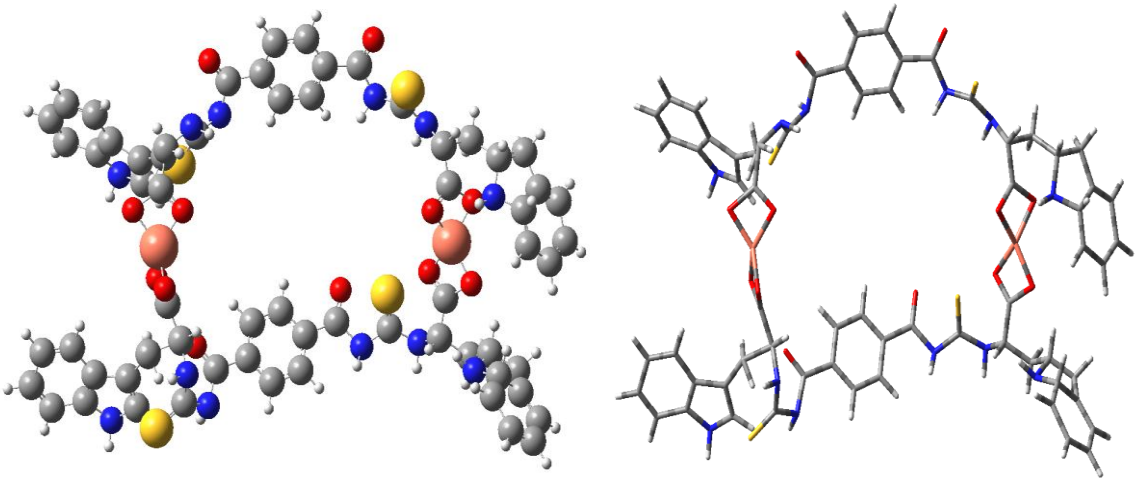

Figure 21 Molecular structure and optimize for L-tryptophane derivative-Cu.

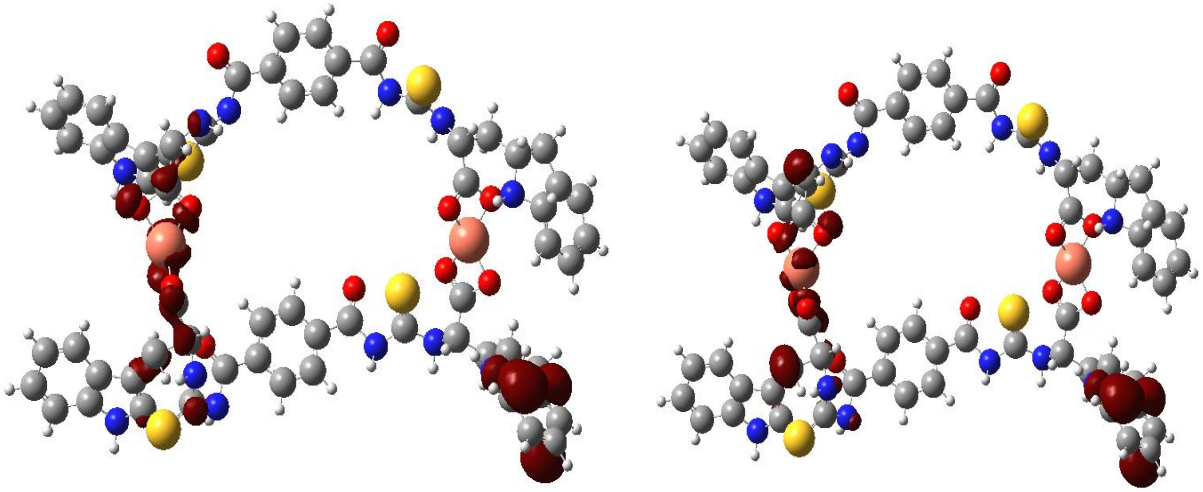

Figure 22 Molecular orbitals HOMO at right and LUMO at left for L-tryptophane derivative-Cu.

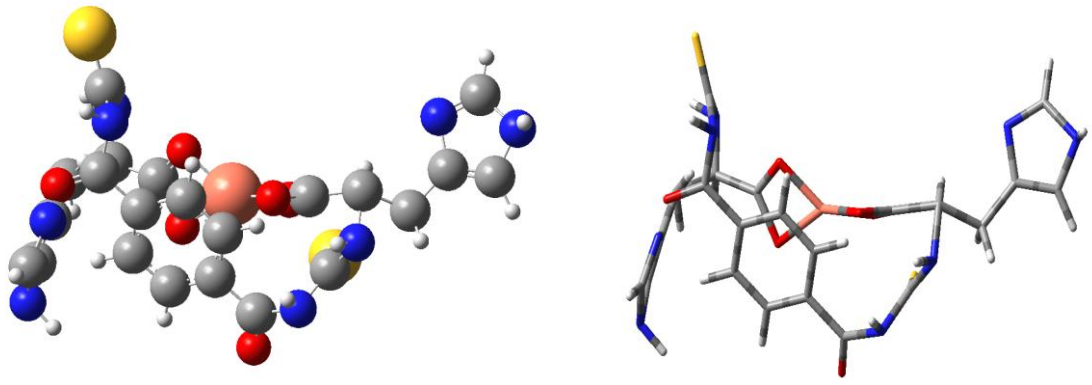

Figure 23 Molecular structure and optimize for L-Histidine derivative-Cu.

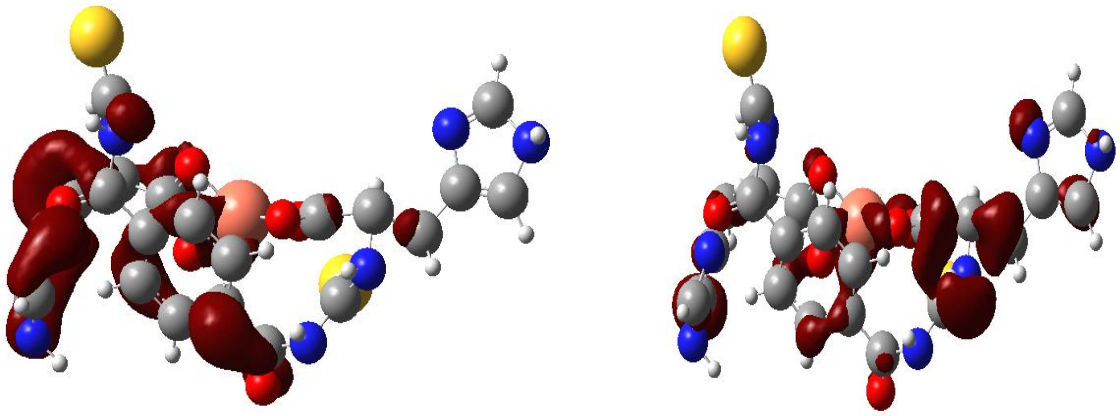

Figure 24 Molecular orbitals HOMO at right and LUMO at left for L-Histidine derivative-Cu.

Conclusions

The present measurements by IR, ^{1}H NMR, XRD confirm the formation of the amino acid derivative (L-lysine derivative and L-tryptophane derivative and L-alanine derivative) their copper (II) complexes with (2:1), While L-Histidine derivative found that the correlation ratio is (1:1) with copper (II), according to what he gave the results of X-ray diffraction for each of the ligands and complexes. The DFT theoretical study provided critical insights into the structural, electronic, and reactive properties of the synthesized amino acid–terephthaloyl isothiocyanate (TPI) complexes.

DFT-optimized structures confirmed the proposed binding modes, with TPI acting as a bridging ligand between amino acids via hydrogen bonds and/or coordination interactions. Calculated bond lengths and angles agreed with experimental data (e.g., XRD, FTIR), validating the proposed complexation. HOMO-LUMO analysis revealed the energy gap (ΔE), indicating the complexes' chemical stability and charge-transfer behavior and the HOMO-LUMO gap will be used as a tool to predict the stability and reactivity of the copper (II) amino acid complexes. Large gap good for stability for pharmaceutical applications while small gap favors catalytic and redox processes. These, in summary, are the guiding factors toward the rational design of copper complexes with properties tailor-made for precise chemical or biological functions. Global reactivity descriptors (electronegativity, chemical hardness/softness, electrophilicity) predicted the complexes' reactivity trends, supporting experimental observations. NCI (Non-Covalent Interaction) analysis and AIM (Atoms in Molecules) theory highlighted the role of hydrogen bonds (N–H···O=C, C–H···S) and van der Waals forces in stabilizing the complexes. TPI–amino acid–Cu(II) complexes are promising in catalysis, medicine, and material science. However, the most important aspect is to overcome the synthetic and characterization challenges. The priorities of future work should be:

A. Structural precision: Advanced diffraction/spectroscopic techniques.

B. Biological validation: In vivo toxicity studies.

C. Industrial scalability: Green synthesis routes.

These systems could bridge the gap between bioinorganic chemistry and functional materials so long as the disadvantages are systematically addressed.

Acknowledgements

The authors gratefully acknowledge University of Basrah, Iraq for providing laboratory facilities and instrumentation.

Declaration of Generative AI and AI-Assisted Technologies in the writing process

This work was prepared without the use of any generative AI tools, in compliance with journal guidelines.

CRediT Author Statement

Nahed Hazim Al-Haidery: Conceptualization, Methodology, Investigation, Formal analysis, Writing – Original Draft, Writing – Review & Editing. **Hanan Abduljaleel Al-Hazam**: Synthesis, Data Curation, Validation, Writing – Original Draft. **Nuha Hussain Al-Saadawy**: DFT Calculations, Theoretical Analysis, Visualization, Writing – Review & Editing.

All authors contributed to the interpretation of results, manuscript revision, and approval of the final version.

References

[1] SA Aly, SS Hassan, HA El-Boraey, A Eldourghamy, EM Abdalla, FM Alminderej and HH Elganzory. Synthesis, biological activity, and the effect of ionization radiation on the spectral, XRD, and TGA analysis of Cu (I), Cu (II), Zn (II), and Cd (II) complexes. *Arabian Journal for Science and Engineering* 2024; **49(1)**, 361-379.

[2] A Ashraf, MG El-Desouky and M El-Afify. Thermal and spectroscopic studies of some prepared metal complexes and investigation of their potential anticancer and antiviral drug activity against SARS-CoV-2 by molecular docking simulation. *Biointerface Research in Applied Chemistry* 2021; **12**, 1053-1075.

[3] L Peng, H Wang and C Guo. Copper-catalyzed enantioselective difluoromethylation of amino acids via difluorocarbene. *Journal of the American Chemical Society* 2021; **143(17)**, 6376-6381.

[4] S Zehra, T Roisnel and F Arjmand. Enantiomeric amino acid schiff base copper (II) complexes as a new class of RNA-targeted metallo-intercalators: Single X-ray crystal structural details, comparative *in vitro* DNA/RNA binding profile, cleavage, and cytotoxicity. *ACS Omega* 2019; **4(4)**, 7691-7705.

[5] MS Refat, Q Mohsen, AMA Adam, and HH Eldaroti. Synthesis and characterization of complexes formed by Fe (III), Cr (III), Co (II), Cu (II), Cd (II), and Ag (I) ions with the drug captopril and the amino acid glycine. *Bulletin of the Chemical Society of Ethiopia* 2025; **39(6)**, 1137-1152.

[6] L Wei, Q Zhu, SM Xu, X Chang and CJ Wang. Stereodivergent synthesis of α, α-disubstituted α-amino acids via synergistic Cu/Ir catalysis. *Journal of the American Chemical Society* 2018; **140(4)**, 1508-1513.

[7] E Pahonțu, CED Pîrvu, DC Vișan, LI Socea, TV Apostol, C Oprean, V Păunescu, A Ungurianu, DM Marginǎ, I Codiță, S Dumitrescu, D Drăgănescu and G Lupașcu. Evaluation of antimicrobial, antitumor, antioxidant activities, and molecular docking studies of some Co (II), Cu (II), Mn (II), Ni (II), Pd (II), and Pt (II) complexes with a schiff base derived from 2-chloro-5-(trifluoromethyl) aniline. *Applied Organometallic Chemistry* 2025; **39(2)**, 7829.

[8] Y Aimene, 2019. Synthèse et étude physico-chimique des complexes de rhénium (I) avec des ligands contenant le pharmacophore sulfonamide: Approche expérimentale et théorique. Ph. D. Disserttation. University of Guelma, Guelme, Algeria.

[9] D Loreto, G Ferraro and A Merlino. Protein-metallodrugs interactions: Effects on the overall protein structure and characterization of Au, Ru and Pt binding sites. *International Journal of Biological Macromolecules* 2020; **163**, 970-976.

[10] A Merlino. Recent advances in protein metalation: Structural studies. *Chemical Communications* 2021; **57(11)**, 1295-1307.

[11] ME Cucciolito, A D'Amora, GD Feo, G Ferraro, A Giorgio, G Petruk, DM Monti, A Merlino and F Ruffo. Five-coordinate platinum (II) compounds containing sugar ligands: Synthesis, characterization, cytotoxic activity, and interaction with biological macromolecules. *Inorganic Chemistry* 2018; **57(6)**, 3133-3143.

[12] N Asadi, M Ramezanzadeh, G Bahlakeh and B Ramezanzadeh. Theoretical MD/DFT computer explorations and surface-electrochemical investigations of the zinc/iron metal cations interactions with highly active molecules from Lemon balm extract toward the steel corrosion retardation in saline solution. *Journal of Molecular Liquids* 2020; **310**, 113220.

[13] RA Shaw. The completeness properties of Gaussian-type orbitals in quantum chemistry. *International Journal of Quantum Chemistry* 2020; **120(17)**, 26264.

[14] J McClain, Q Sun, GKL Chan and TC Berkelbach. Gaussian-based coupled-cluster theory for the ground-state and band structure of solids. *Journal of Chemical Theory and Computation* 2017; **13(3)**,1209-1218.

[15] F Pereira, K Xiao, DA Latino, C Wu, Q Zhang and JA Sousa. Machine learning methods to predict density functional theory B3LYP energies of HOMO and LUMO orbitals. *Journal of Chemical Information and Modeling* 2017; **57(1)**, 11-21.

[16] FN Ajeel, AM Khudhair and AA Mohammed. Density functional theory investigation of the physical properties of dicyano pyridazine molecules. *International Journal of Science and Research* 2015; **4(4)**, 2334-2339.

[17] FN Ajeel. Analytical insight into the effect of electric field on molecular properties of Homonuclear Diatomic Molecules. *Current Smart Materials* 2017; **2(2)**, 53-61.

[18] AS Alwan, SK Ajeel and ML Jabbar. Theoretical study for Coronene and Coronene-Al, B, C, Ga, In and Coronene-O interactions by using Density Functional theory. *Univesity of Thi-Qar Journal* 2019; **14(4)**, 1-14.

[19] AH Al-Taher, HK Mejbel, LF Al-Badry and WS Abdul-Hassan. Influence of end groups (4F, 4Br, 4CF3, and 4CBr3) of non-fullerene acceptor molecules on the performance of organic solar cells. *The Journal of Nanoparticle Research* 2025; **27(4)**, 96.

[20] FH Hanoon, ML Jabbar and AS Alwan. Effect of thickness on the fractal optical modulator for MgF2, LiF, AL2O3 materials by testing modulation transfer function (MTF). *Journal of Education for Pure Science* 2017; **7(4)**, 168-182.

[21] EK Hamd, AS Alwan and IK Irthiea. Study the effect of welding heat input on the microstructure, hardness, and impact toughness of AISI 1015 steel. *Al-Khwarizmi Engineering Journal* 2018; **14(1)**, 118-27.

[22] AS Alwan. Density functional theory investigation of (C4H2N2) 3 nanocluster and (C4H2N2) 3--P, Al, As, B, C and in nanoclusters. *AIP Conference Proceedings* 2020; **2292(1)**, 030013.

[23] M Pervaiz, I Ahmad, M Yousaf, S Kirn, A Munawar, Z Saeed, A Adnan, T Gulzar, T Kamal, A Ahmad and A Rashid. Synthesis, spectral and antimicrobial studies of amino acid derivative schiff base metal (Co, Mn, Cu, and Cd) complexes. *Spectrochimica Acta Part A: Molecular and Biomolecular Spectroscopy* 2019; **206**, 642-649.

[24] A Wojciechowska, J Janczak, W Zierkiewicz, P Rytlewski, T Rojek and M Duczmal. Copper (II) complex with L-arginine–crystal structure, DFT calculations, spectroscopic, thermal and magnetic properties. *Materials Chemistry and Physics* 2019; **228**, 272-284.

[25] N Chetry, TG Devi and T Karlo. Synthesis and characterization of metal complex amino acid using spectroscopic methods and theoretical calculation. *Journal of Molecular Structure* 2022; **1250**, 131670.

[26] GV Gurskaya. *The molecular structure of amino acids: Determination by X-ray diffraction analysis*. Springer Science & Business Media, Academy of Sciences of the USSR, Moscow, Russia, 2012.

[27] W Nbili, M Runde, RA Timothy, F Lefebvre, W Kamisky, CB Nasr and K Kaabi. Investigation on X-ray diffraction, IR, UV-visible, fluorescence, thermogravimetric, DFT studies, and molecular docking approach of a new $C_6H_{17}\cdot_{16}Cl_3CuN_3O_{0.58}$ complex. *Journal of Molecular Structure* 2025; **1326**, 141049.